Electronic Supplementary Material (ESI) for Chemical Communications.

Nickel(II)-Methyl Complexes Adopting Unusual Seesaw Geometries

Supplementary Information

Ethan A. Hill[†], Norman Zhao[†], Alexander S. Filatov, John S. Anderson*

Department of Chemistry, University of Chicago, Chicago, Illinois 60637, United States

Correspondence to: jsanderson@uchicago.edu

Table of Contents

Materials and Instrumentation

All manipulations were performed under a dry nitrogen atmosphere using either standard Schlenk techniques or in an mBraun Unilab Pro glove box unless otherwise stated. All chemicals were obtained from commercial sources and used as received unless otherwise stated. Solvents were dried on a solvent purification system from Pure Process Technologies and passed through a column of activated alumina before storing over 4 Å molecular sieves under N_2. Diethyl ether and tetrahydrofuran (THF) were stirred over NaK alloy and passed through a column of activated alumina prior to storing over 4 Å sieves under N_2. Tetraethylammonium tetrachloronickelate ($[Et_4N]_2[NiCl_4]$), $[PhB(^tBuIm)_3][OTf]_2$, 1-adamantylimidazole, and $[PhB(AdIm)_3][OTf]_2$ were prepared according to literature procedures.[1–4]

UV-vis spectra were recorded on a Thermo Scientific Evolution 300 spectrometer with the VISIONpro software suite. IR spectra were recorded on a Bruker Tensor II spectrometer with the OPUS software suite. NMR spectra for ^1H, $^{13}C\{^1H\}$, and $^{11}B\{^1H\}$ were recorded on either Bruker DRX-400 or AVANCE-500 spectrometers. ^1H and $^{13}C\{^1H\}$ spectra were referenced to residual solvent peaks. Combustion analysis was performed by Midwest Microlab. Magnetic moments were determined using the Evans method.[5]

Complex Synthesis and Characterization

*$PhB(^tBuIm)_3Ni^{II}Cl$ (**1a**):* To a Schlenk flask was added proligand $[PhB(^tBuIm)_3][OTf]_2$ (5.00 g, 6.59 mmol) and THF (100 mL). In a separate Schlenk flask, $^iPr_2NH$ (2.6 mL, 20.1 mmol) was added to THF (30 mL). Both Schlenk flasks were sealed with rubber septa, brought out of the glovebox, attached to a Schlenk line, and cooled to –78 ºC using a dry ice/isopropanol bath. A solution of ^{n}BuLi (8.1 mL, 20.1 mmol, 2.5 M in hexanes) was then added to the solution of iPr_2NH to generate lithium diisopropylamide (LDA) *in situ*. The solution of LDA in THF was then transferred via cannula to a cold suspension of the proligand. The reaction mixture was stirred at –78 ºC for approximately 45 minutes, and then solid $[Et_4N]_2[NiCl_4]$ (2.87 g, 6.92 mmol) was added under positive nitrogen pressure. After stirring at room temperature overnight, the brown reaction mixture was concentrated under vacuum to yield a green/brown residue. The flask was returned to a glovebox and triturated with hexanes (30 mL) and dried once more under vacuum. The residue was extracted into toluene (100 mL) and filtered through a pad of Celite. The resulting green solution was concentrated and redissolved in a minimal amount of toluene before layering under pentane at –35 ºC. Green crystals form after several days which are separated from a flocculent yellow/brown powder by washing with cold pentane. Crystals were dried under vacuum and lyophilized from benzene to yield pure **1a** (1.05 g, 1.90 mmol 29% yield). After separating and drying the mother liquor under vacuum, several successive crystallizations are required to achieve yields varying from 10-29%. Single crystals suitable for X-ray diffraction were grown from liquid diffusion of pentane into a concentrated solution of toluene solution of the complex at –35 ºC over several days. ^1H NMR (400 MHz, C_6D_6) δ 106.31, 15.27, 7.43, 7.26, 6.34. ^{11}B NMR (128 MHz, C_6D_6) δ −9.7. μ_{eff} (C_6D_6): 2.9 μ_B (for S = 1, μ_{SO} = 2.83 μ_B) UV-vis, nm in dichloromethane (ε, M^{-1} cm^{-1}): 446 (166), 718 (228). IR (KBr): 3142 (w), 3076 (w), 3051 (w), 3018 (w), 2978 (s), 2934 (m), 2876 (w), 1478 (w), 1432 (w), 1369 (m), 1333 (m), 1278 (s), 1232 (w), 1207 (s), 1193 (s), 1151 (s), 1123 (m), 1027 (m), 1021 (s), 931 (w), 898 (w), 880 (s), 824 (w), 806 (w), 792 (m), 722

(s), 710 (s), 700 (m), 669 (w). Anal.; Calc. for $C_{27}H_{38}N_6BNiCl$: C 58.79, H 6.94, N 15.24.; C 59.02, H 6.80, N 14.92.

*$PhB(AdIm)_3Ni^{II}Cl$ (**1b**)*: The proligand, $[PhB(AdIm)_3][OTf]_2$, was synthesized in an analogous manner to $[PhB(^tBuIm)_3][OTf]_2$ and its spectroscopic data matched previous literature.[4] To a 250 mL Schlenk flask was added $[PhB(AdIm)_3][OTf]_2$ (4.52 g, 4.55 mmol) and THF (60 mL). In a separate 50 mL Schlenk flask was added ^{i}PrNH (1.43 g, 14.0 mmol) and THF (20 mL). Both flasks were sealed with rubber septa, removed from the glovebox, and attached to a Schlenk line before cooling to −78 °C using a dry ice/isopropanol bath. After cooling, a solution of nBuLi (5.6 mL, 2.5 M in hexanes) was added via syringe to the cold ^{i}PrNH solution to generate LDA *in situ*. After briefly stirring (~5 min) the solution of LDA was transferred via cannula to a the cooled solution of $[PhB(AdIm)_3][OTf]_2$ and the mixture stirred for 1 h at −78 °C whereupon a turbid, peach-colored solution results. Under a positive flow of N_2, the septum was quickly removed and solid $[Et_4N]_2[NiCl_4]$ (2.10 g, 4.55 mmol) was added in one portion before replacing the septum. The mixture was stirred overnight and allowed to slowly warm to room temperature. The resulting brown solution was dried under vacuum at 50 °C for 1 h before returning to a glovebox. The brown residue was triturated once with hexanes (50 mL) before drying once more under vacuum. A brown, chalky residue results which is washed with several portions of room temperature toluene (typically ~50 mL in total) until a green solid remains. The green solid is transferred to a 125 mL Erlenmeyer flask and treated with hot toluene (100 °C, ~50-100 mL in total) until a green solution separates from a gray, oily solid (sometimes pale blue due to unreacted $[Et_4N]_2[NiCl_4]$). The mixture is filtered hot through a pad of Celite before drying to a green residue under vacuum. The resulting residue is dissolved in a minimum of dichloromethane (DCM) before layering under pentanes and storing at −35 °C for several days to yield dark green crystalline blocks (833 mg, 1.06 mmol, 23% yield). After separating and drying the mother liquor under vacuum, several successive crystallizations are required to achieve yields varying from 15-23%. ^{1}H NMR (400 MHz, CD_2Cl_2) δ 103.84, 13.85, 7.55-7.52, 3.79, 1.54. ^{11}B NMR (128 MHz, C_6D_6) δ −11.3. μ_{eff} (CD_2Cl_2): 3.0 μ_B (for S = 1, μ_{SO} = 2.83 μ_B) UV-vis, nm in THF (ε, M^{-1} cm^{-1}): 360 (532) 450 (171), 720 (312) 835 (sh, 80). IR (KBr): 3153 (w), 3041 (w), 2903 (s), 2847 (s), 2667 (w), 1654 (w), 1544 (w), 1454 (m), 1404 (m), 1390 (m), 1326 (m), 1277 (m), 1239 (m), 1183 (s), 1163 (s), 1125 (m), 1103 (m), 1073 (w), 1019 (s), 880 (s), 835 (m), 790 (m), 735 (m), 713 (s), 695 (m), 645 (w), 625 (w). Anal.; Calc. for $C_{45}H_{56}N_6BNiCl$: C 68.77, H 7.18, N 10.69; C 68.92, H 7.40, N 10.20.

*$PhB(^tBuIm)_3Ni^{II}Me$ (**2a**):* A solution of methyllithium (1.6 M in diethyl ether, 250 µL, 0.40 mmol) was added to a suspension of **1** (200 mg, 0.36 mmol) in diethyl ether (10 mL) at room temperature. After stirring for 30 minutes, the dark red mixture was filtered through a pad of Celite and concentrated under reduced pressure. The residue was washed with hexanes (3 x 5 mL) and dried once more under vacuum to yield a red-orange powder (71 mg, 0.13 mmol, 37% yield). Crystals suitable for X-ray diffraction were grown in a concentrated solution of diethyl ether at –35 ºC. ^{1}H NMR (400 MHz, C_6D_6) δ 8.30 (d, Ph, 2H), 7.48 (t, Ph, 2H), 7.39 (t, Ph, 1H), 7.28 (s, Im, 3H), 6.52 (s, Im, 3H), 1.60 (s, ^{t}Bu, 27H), 1.25 (br s, Me, 3H). Note that the Ni-CH_3 resonance displays solvent dependence, shifting from 1.25 ppm in C_6D_6, to 0.89 ppm in d_8-toluene, and 0.29 ppm in d_8-THF. ^{11}B NMR (128 MHz, C_6D_6) δ 1.4. ^{13}C NMR (126 MHz, C_6D_6) δ 144.2, 135.4, 127.4, 124.9, 116.6, 55.9, 31.5. UV-vis in THF: trailing UV absorbances (see below). IR (KBr): 3139 (w), 3049 (w), 2975 (s), 2925 (m), 2873 (w), 1650 (m), 1636 (m), 1475 (w), 1433 (m), 1398 (m), 1370 (m), 1337 (m), 1267 (m), 1194 (s), 1150 (m), 1110 (m), 1109 (m), 1030 (m), 931 (w), 876

(m), 826 (s), 792 (s), 737 (s), 707 (s), 638 (w). Several attempts at obtaining suitable elemental analysis data were unsuccessful. This is attributed to either incomplete drying or decay during shipping and handling, both as a result of the thermal instability of the complex.

*PhB(AdIm)$_3$Ni^{II}Me (**2b**)*: In a 20 mL scintillation vial, **1b** (200 mg, 0.25 mmol) was dissolved in THF (10 mL). To this solution was added MeLi (225 μL, 0.36 mmol, 1.6 M solution in diethyl ether) via microsyringe. The solution was stirred for 2 h, during which time a color change from green to red occurs. The solution was dried to a red-brown residue under vacuum and extracted into toluene (15 mL) before filtering through a pad of Celite. The resulting dark red solution was layered under hexamethyldisiloxane and stored at −35 °C to yield a dark red, microcrystalline solid (99 mg, 0.13 mmol, 51% yield). Single crystals suitable for XRD were grown from toluene layered under pentane at −35 °C. ^{1}H NMR (400 MHz, C_6D_6) δ 8.34 (d, Ph, 2H), 7.50 (t, Ph, 2H), 7.41 (m, Ph, 1H), 7.30 (d, Im, 3H), 6.58 (s, Im, 3H), 2.42 (s, Ad, 18H), 2.09 (s, Ad, 9H), 1.65 (m, Ad, 18H), 1.05 (br s, Me, 3H). ^{11}B NMR (128 MHz, C_6D_6) δ 1.2. ^{13}C NMR (126 MHz, C_6D_6) δ 135.4, 128.2, 127.4, 124.4, 115.2, 56.2, 44.4, 36.7, 30.5. UV-vis in THF: broad shoulders and trailing UV absorbances (see below). IR (KBr): 3136 (w), 3060 (w), 2908 (s), 2852 (s), 2680 (w), 1644 (s), 1478 (w), 1451 (m), 1431 (w), 1398 (m), 1376 (w), 1357 (w), 1331 (m), 1307 (m), 1283 (m), 1240 (m), 1186 (m), 1169 (m), 1129 (w), 1104 (w), 1052 (w), 1026 (w), 876 (m), 835 (s), 792 (s), 736 (m), 703 (m), 680 (m). Several attempts at obtaining suitable elemental analysis data were unsuccessful. This is attributed to either incomplete drying or decay during shipping and handling, both as a result of the thermal instability of the complex.

Experimental Procedures

Crystallographic Details: The diffraction data for **2b** were measured at 110 K on a Bruker D8 fixed-chi with PILATUS1M (CdTe) pixel array detector (synchrotron radiation, $\lambda = 0.41328$ Å (30 KeV)) at the Chem-MatCARS 15-ID-B beamline at the Advanced Photon Source (Argonne National Laboratory). The diffraction data for **1a,1b,** and **2a** were measured at 100 K on a Bruker D8 VENTURE diffractometer equipped with a microfocus Mo-target X-ray tube ($\lambda = 0.71073$ Å) and PHOTON 100 CMOS detector. Data reduction and integration were performed with the Bruker APEX3 software package (Bruker AXS, version 2017.3-0, 2018). Data were scaled and corrected for absorption effects using the multi-scan procedure as implemented in SADABS (Bruker AXS, version 2014/5).[6] The structures were solved by SHELXT (Version 2014/5) and refined by a full-matrix least-squares procedure using OLEX2 (XL refinement program version 2018/1).[7–9]

Computational Methods: Geometry optimizations were performed using the ORCA program suite.[10] The O3LYP hybrid functional was used for all calculations, unless otherwise specified. The basis sets for each atom were as follows: def2-TZVPP for Ni, N, and carbene C; def2-SVP for B, H, and remaining C.[11–13] A full frequency calculation was performed on the optimized seesaw geometry of **2a** to ensure that there were no imaginary frequencies and ensure true minima in the energies. This geometry was then optimized as a triplet to obtain the linearized geometry, which was used to generate the molecular orbitals (Figure 2 and S16) and geometry scan for the lever mechanism (Figure S17). The initial geometries were generated using crystallographic data. The geometry plots were created from the optimized xyz cartesian coordinates in Diamond 3.2.[14]

The free energies of the respective species are shown in Table S3. The Kohn-Sham molecular orbitals were plotted in Avogadro with ISO values for the surface set at 0.09.[15]

Calculation of $\Delta G^{\ddagger}$ from variable temperature ^1H NMR spectroscopy: A method for determining activation barriers to exchange processes between two inequivalent species has previously been described.[16] Using this method, two different activation barriers are calculated for the two inequivalent species in solution. In this case these two species are in fact topomers, distinguished only by arbitrarily assigning the three NHC groups and changing the orientation of the methyl ligand from between one pair to a neighboring pair. For simplicity, only one set of the coalescence temperatures and $\Delta G^{\ddagger}$ values were reported in the text where the $\Delta G^{\ddagger}$ value was calculated as the average of the A and B components with the standard deviation used as an estimate of the error. Below are the data for a total of three different resonances of each species reported here for completeness. The equation shown was used to calculate the $\Delta G^{\ddagger}$ values where Tc = coalescence temperature, X and ΔP (0.67) are related to the difference in population of the doublet,[17] and $\Delta\nu$ = difference in Hz of the fully resolved doublet of the exchanging species.

$$\Delta G^{\ddagger} = 4.575 * 10^{-3} * Tc * \left(10.62 + \log\left(\frac{X}{2\pi(1 \pm \Delta P)}\right) + \log\left(\frac{Tc}{\Delta\nu}\right)\right) \qquad (1)$$

2a	**Im (high ppm)**		**Im (low ppm)**		**^{t}Bu**	
	A	B	A	B	A	B
ν (ppm)	7.05	7.42	5.82	6.07	1.83	1.43
ν (Hz)	3526	3711	2908	3037	916	716
$\Delta\nu$ (Hz)	186		130		201	
Tc (K)	212		215		219	
$\Delta G^{\ddagger}_A$ (kcal/mol)	9.8		10.1		10.1	
$\Delta G^{\ddagger}_B$ (kcal/mol)	10.5		10.8		10.8	
Average	10.1		10.4		10.4	
Std Dev	0.5		0.5		0.5	

2b	**Im (high ppm)**		**Im (low ppm)**		**Ad**	
	A	B	A	B	A	B
ppm	7.20	7.38	5.98	6.20	2.64	2.19
Hz	3598	3690	2991	3099	1318	1094
ΔHz	92		108		224	
Tc (K)	219		225		231	
$\Delta G^{\ddagger}_A$ (kcal/mol)	10.4		10.6		10.6	
$\Delta G^{\ddagger}_B$ (kcal/mol)	11.1		11.4		11.3	
Average	10.7		11.0		11.0	
Std Dev	0.5		0.5		0.5	

Table S1: Values extracted from the variable temperature ^{1}H NMR spectra used for calculating the $\Delta G^{\ddagger}$ values for complexes **2a** and **2b**.

Figures and Tables

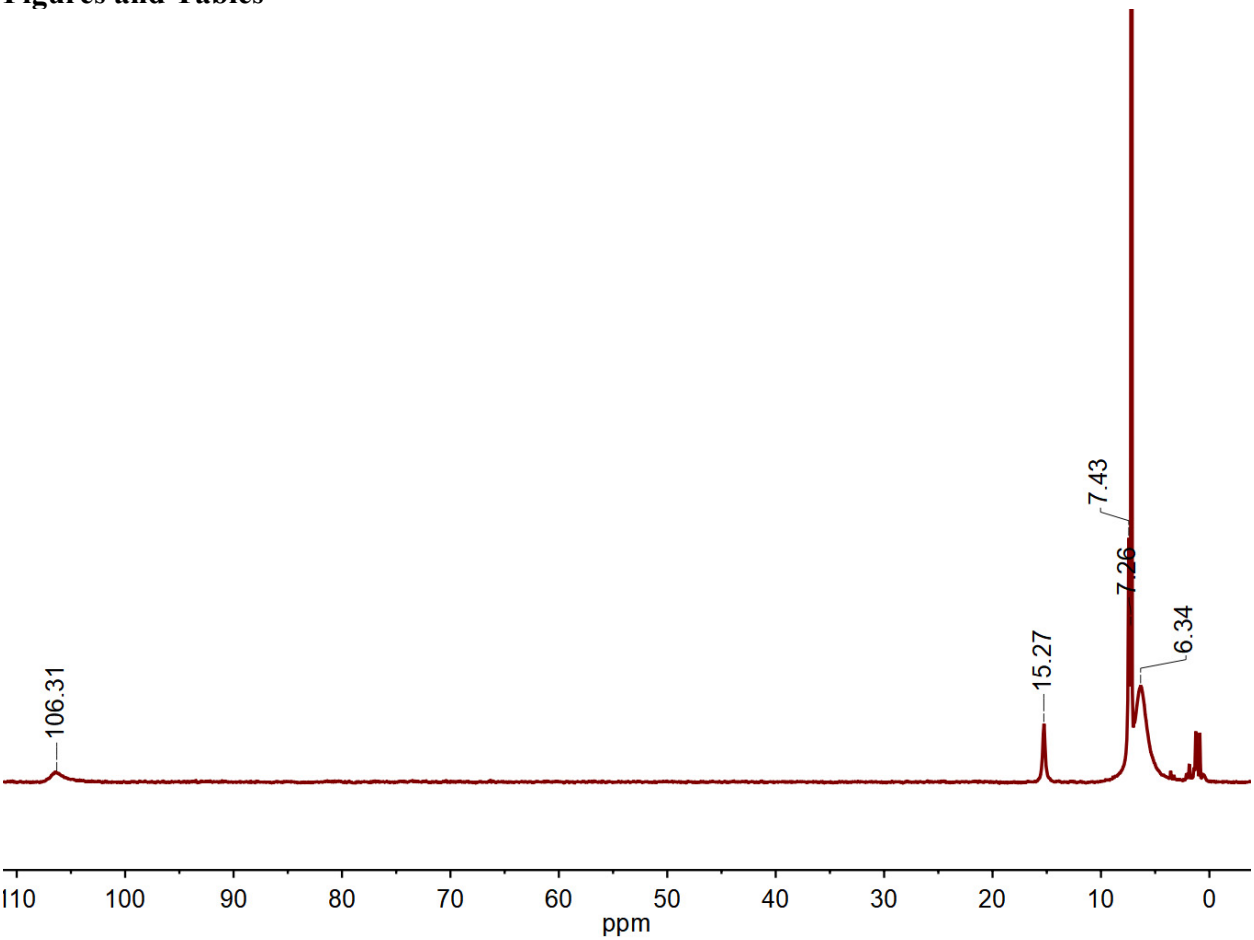

Figure S1. The paramagnetic ^{1}H NMR spectrum of **1a** in C_6D_6 at 298 K. Top of the solvent residual peak has been clipped to more clearly see paramagnetic features.

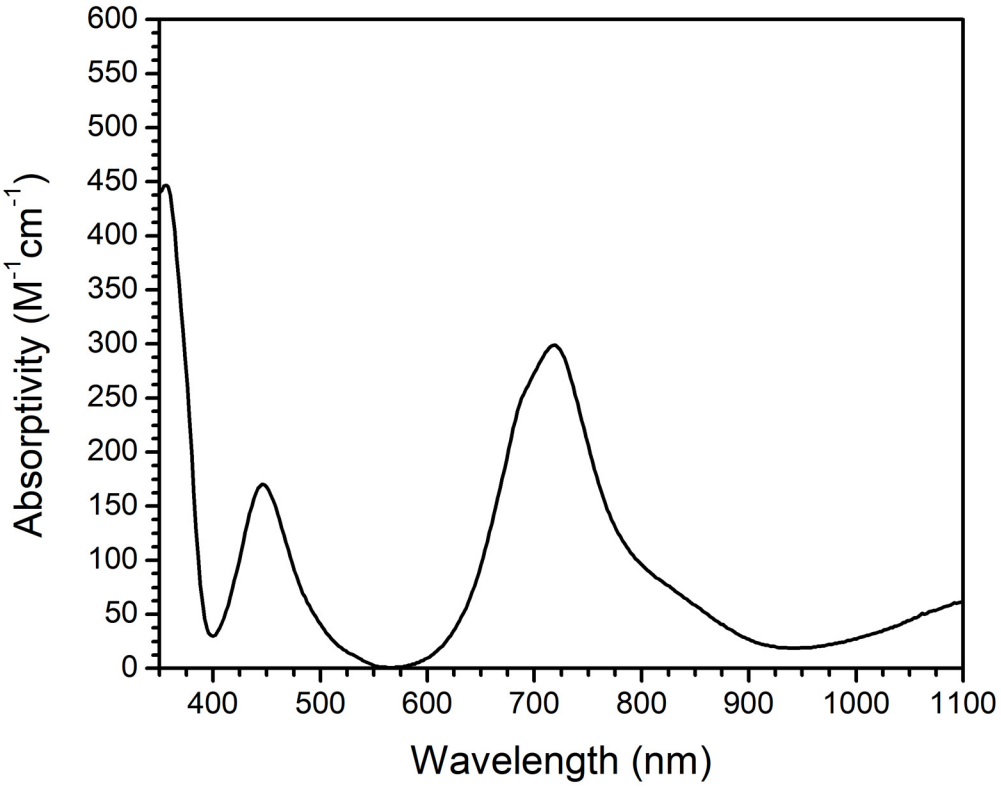

Figure S2. UV-vis spectrum of **1a** in DCM at 298 K.

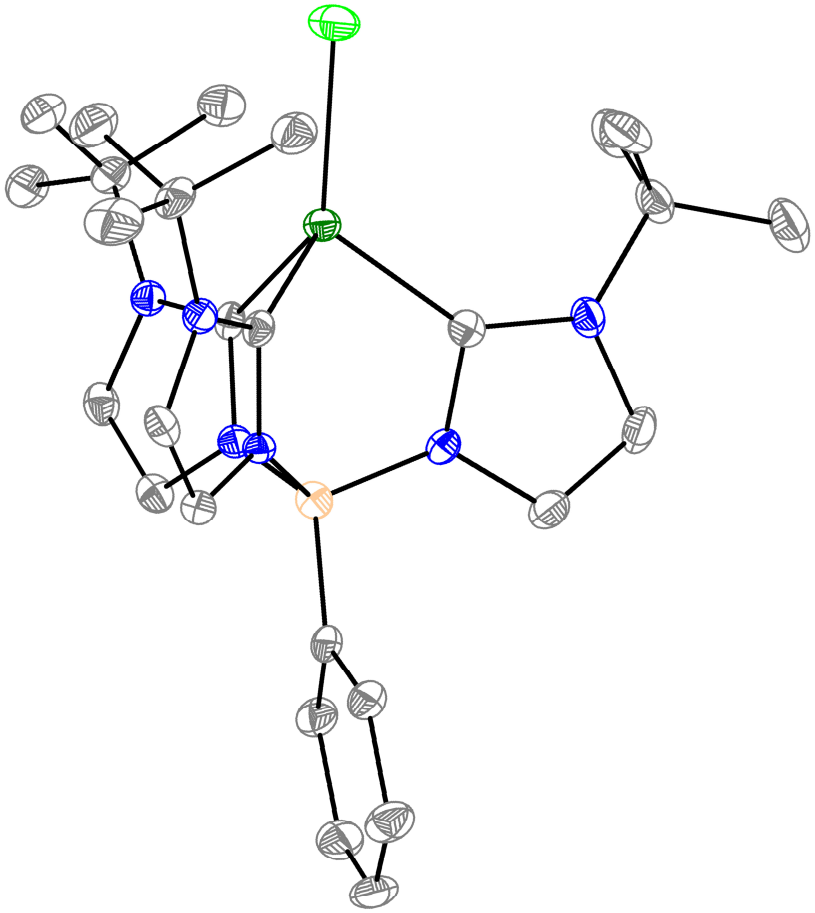

Figure S3. Molecular structure of **1a** determined by single crystal XRD. Ellipsoids drawn at 50% probability, H-atoms and solvent molecules omitted for clarity. Only one molecule in the unit cell is shown. Atom colors are dark green = Ni, light green = Cl, blue = N, tan = B, and gray = C.

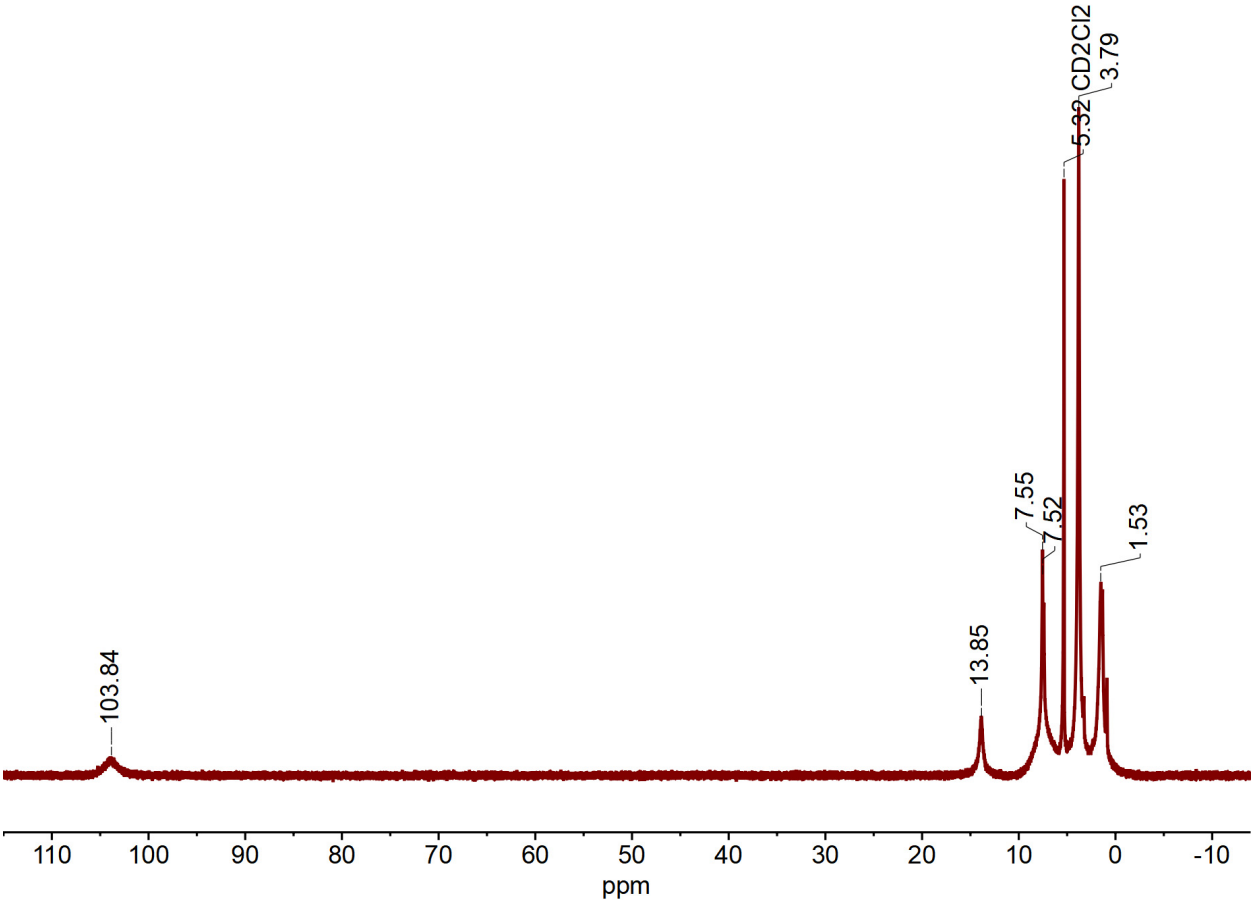

Figure S4. The paramagnetic ^{1}H NMR spectrum of **1b** in CD_2Cl_2 at 298 K.

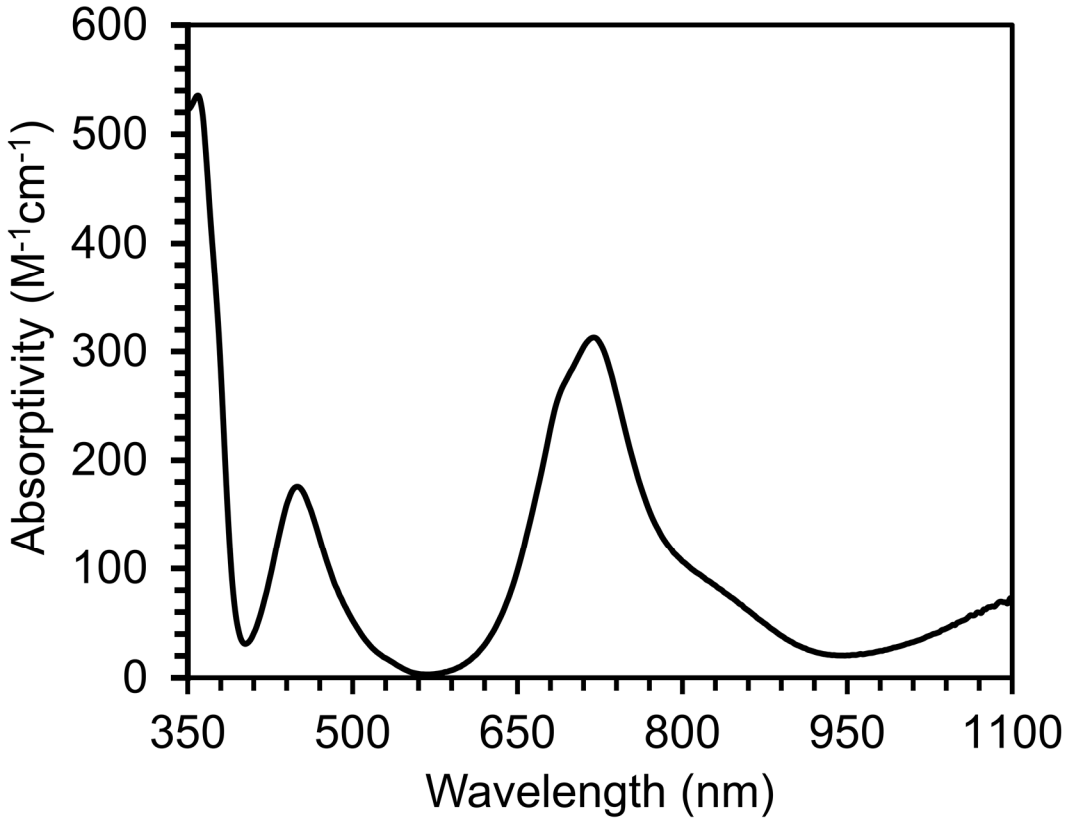

Figure S5. The UV-vis spectrum of **1b** in THF at 298 K.

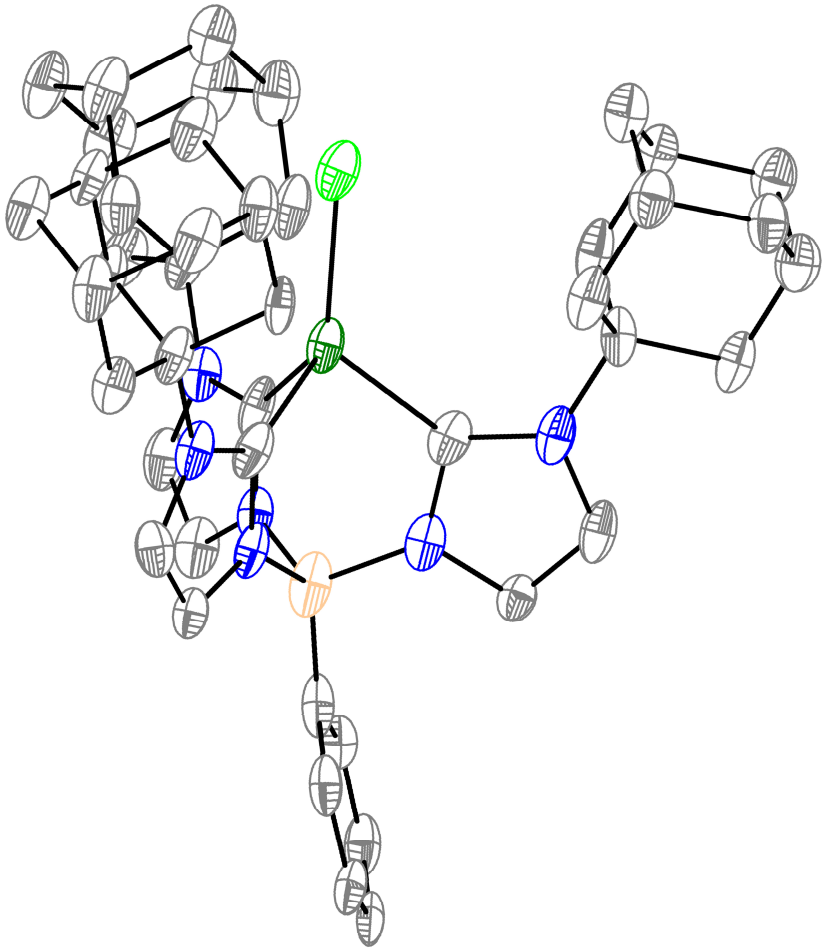

Figure S6. The molecular structure of **1b** determined by single crystal XRD. Ellipsoids drawn at 50% probability, H-atoms and solvent molecules omitted for clarity. Atom colors are dark green = Ni, light green = Cl, blue = N, tan = B, and gray = C.

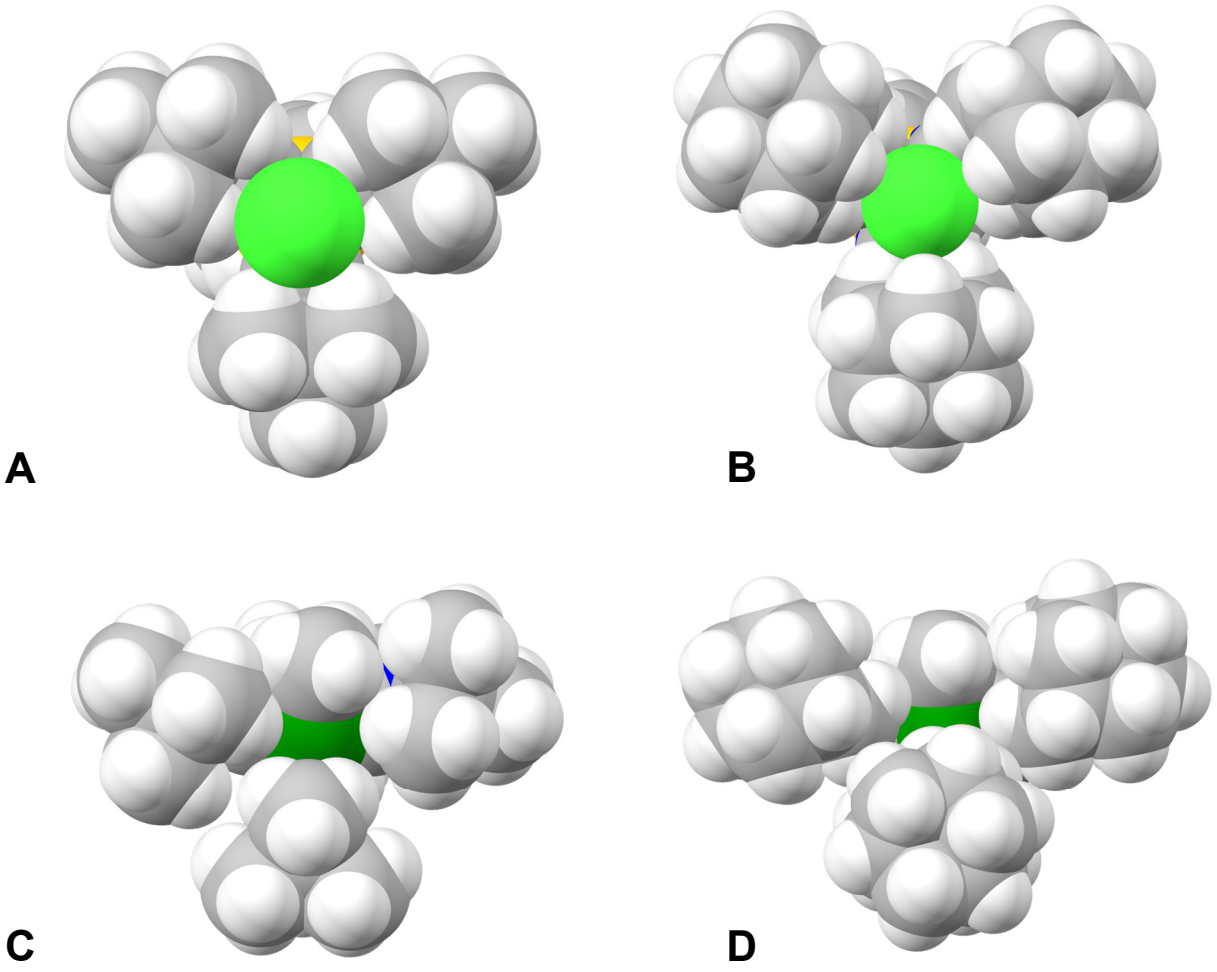

Figure S7. Depiction of the space-filling models of **1a** (A), **1b** (B), **2a** (C), and **2b** (D) to show the distortion around the nickel center due to the change in geometry. Color code: dark green = Ni, light green = Cl, gray = C, white = H, blue = N, tan = B

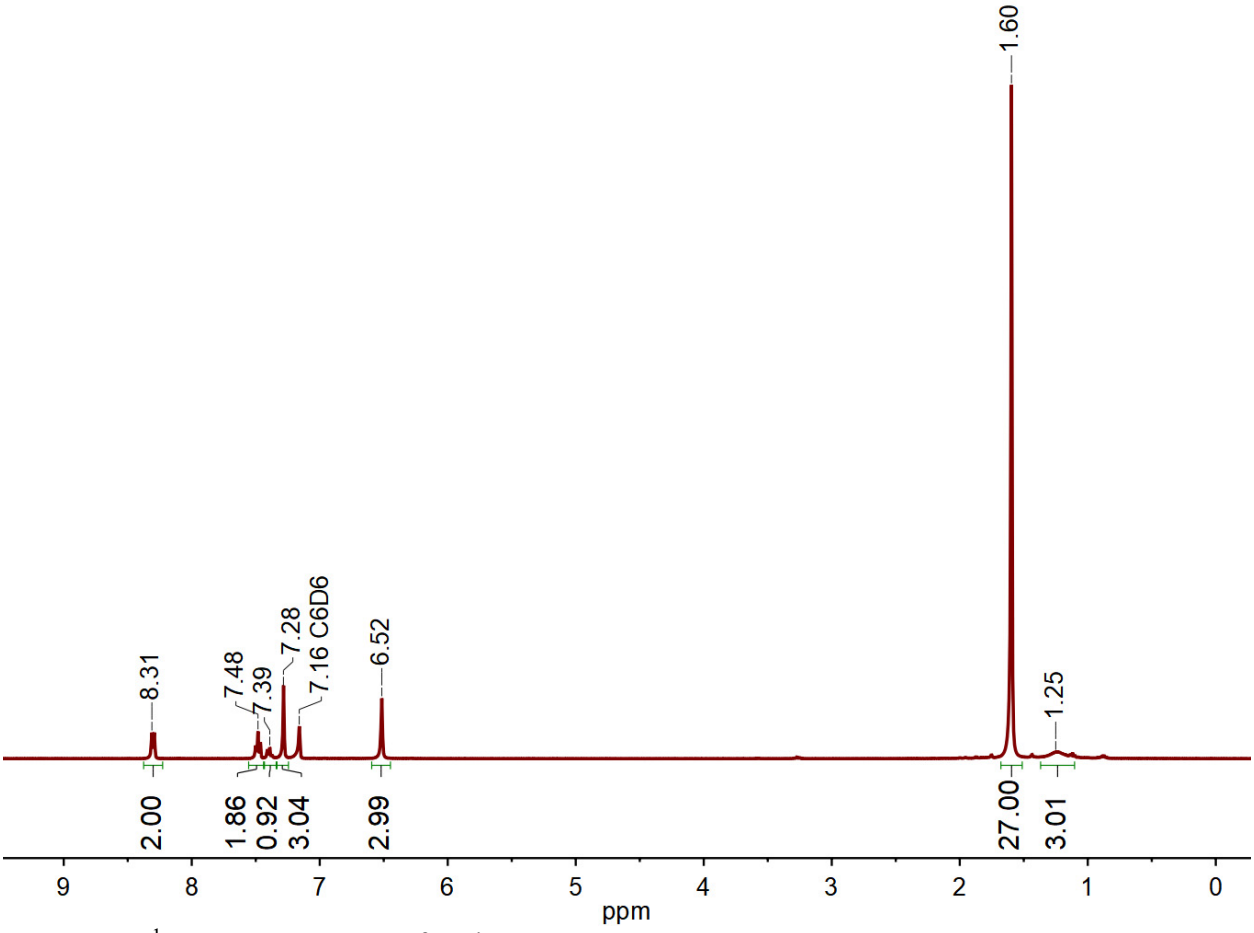

Figure S8. ^{1}H NMR spectrum of **2a** in C_6D_6 at 298 K.

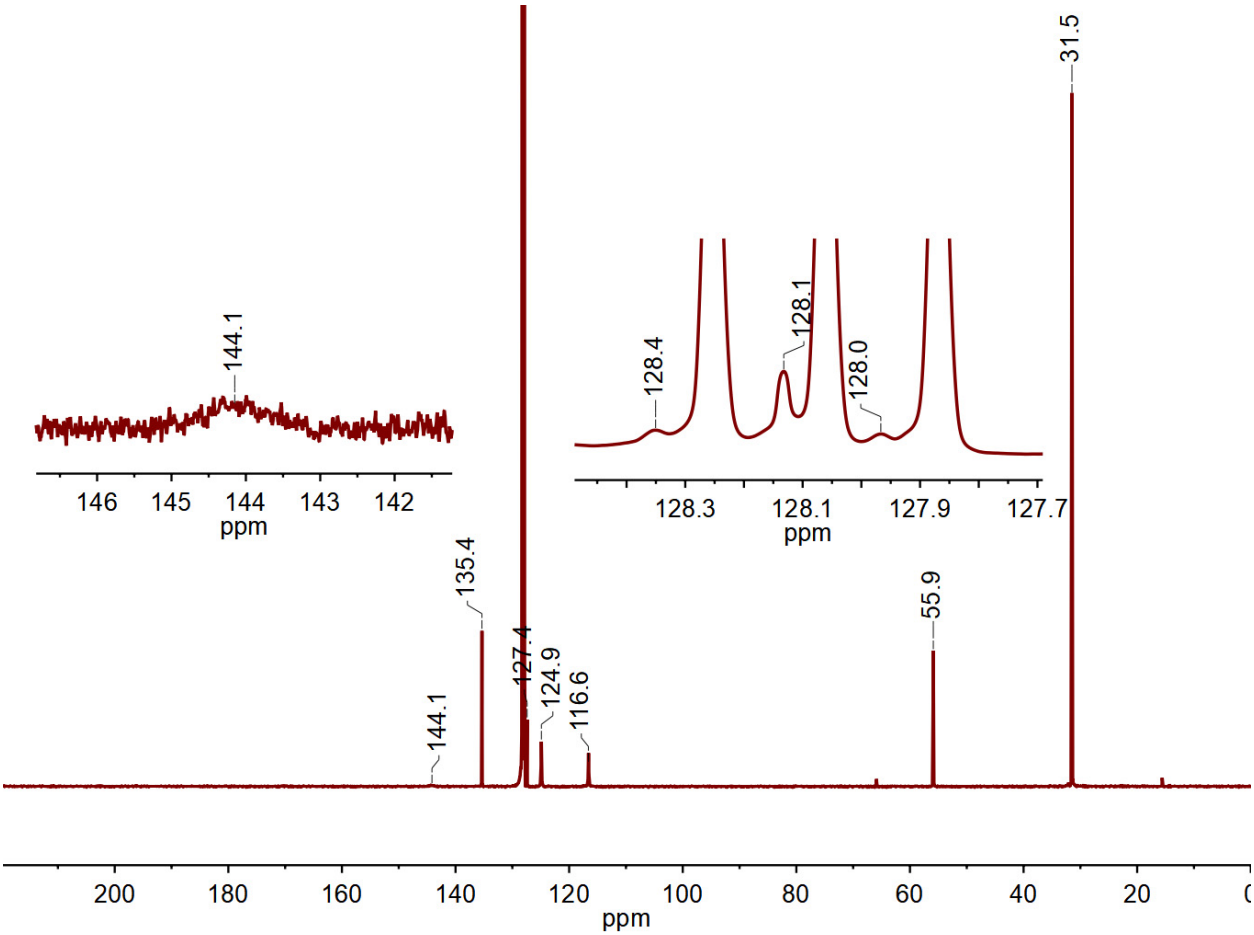

Figure S9. ^{13}C NMR spectrum of **2a** in C_6D_6 at 298 K.

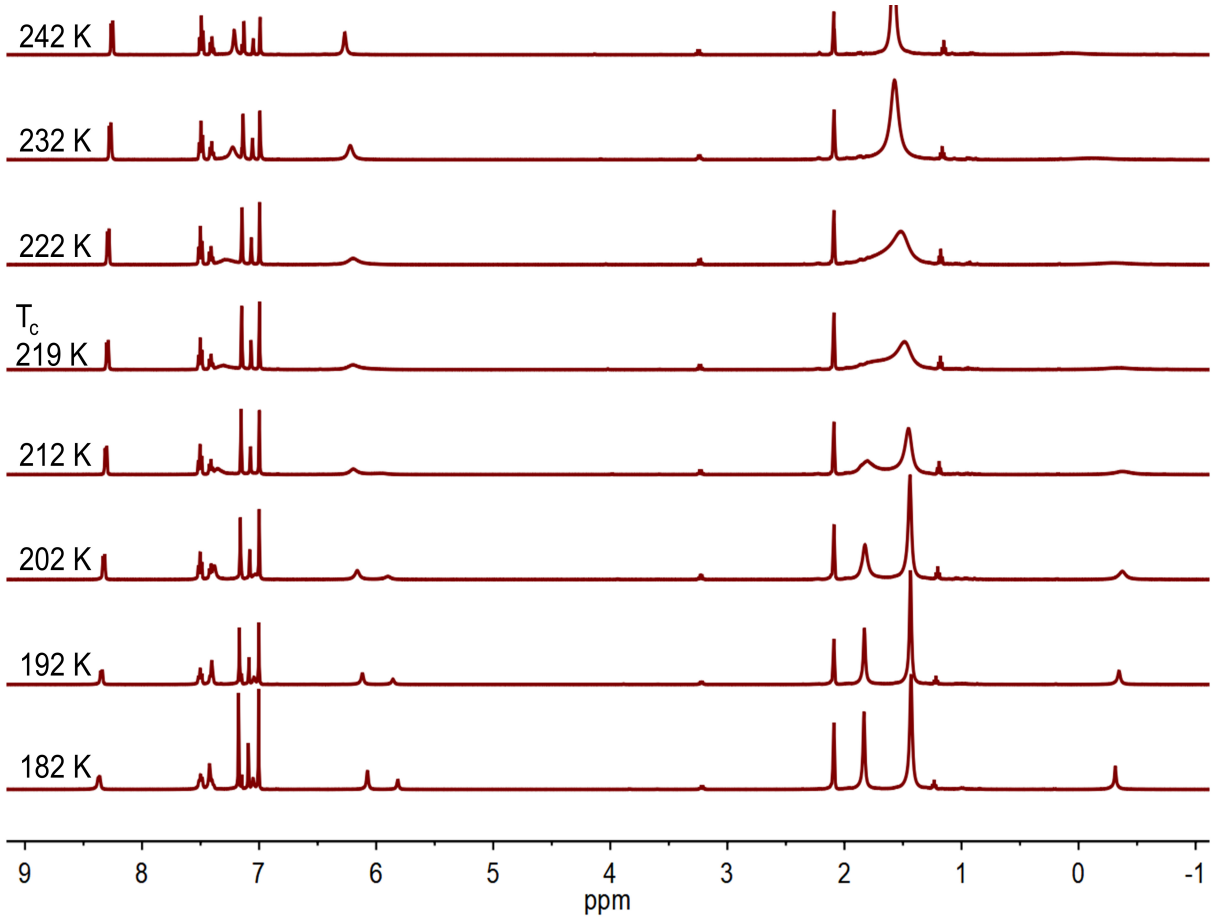

Figure S10. Variable temperature ^{1}H NMR spectra of **2a** in *d*$_8$-toluene. Reproduced here from the main text.

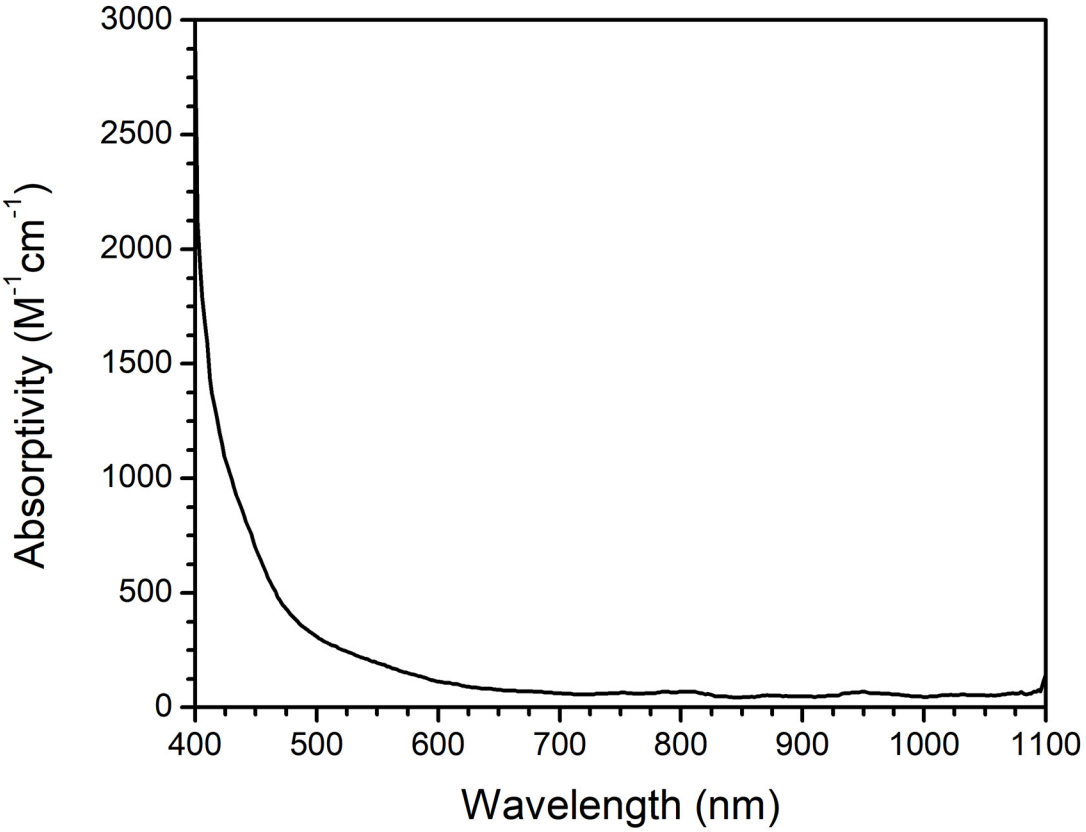

Figure S11. The UV-vis spectrum of **2a** in THF at 298 K.

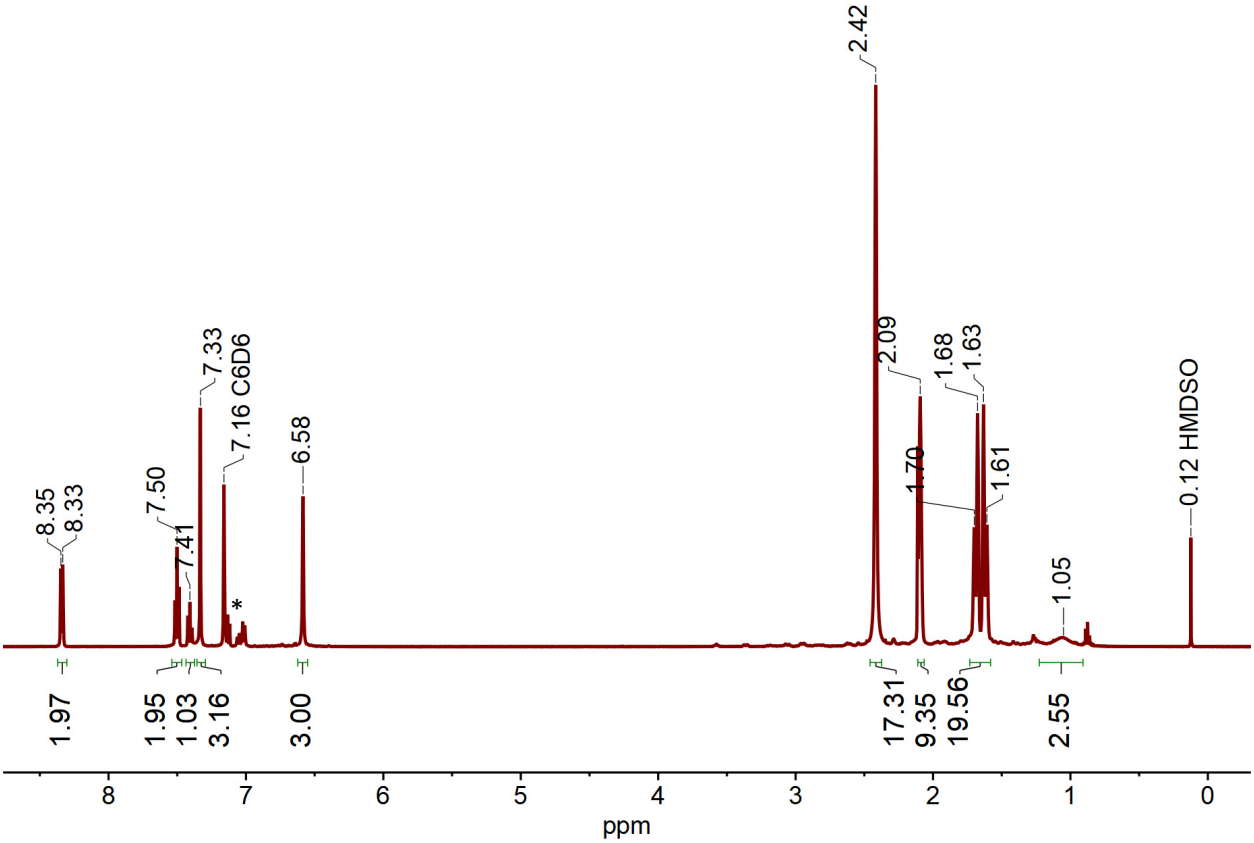

Figure S12. The ^{1}H NMR spectrum of **2b** in C_6D_6 at 298 K. Resonances for residual toluene are marked with an asterisk.

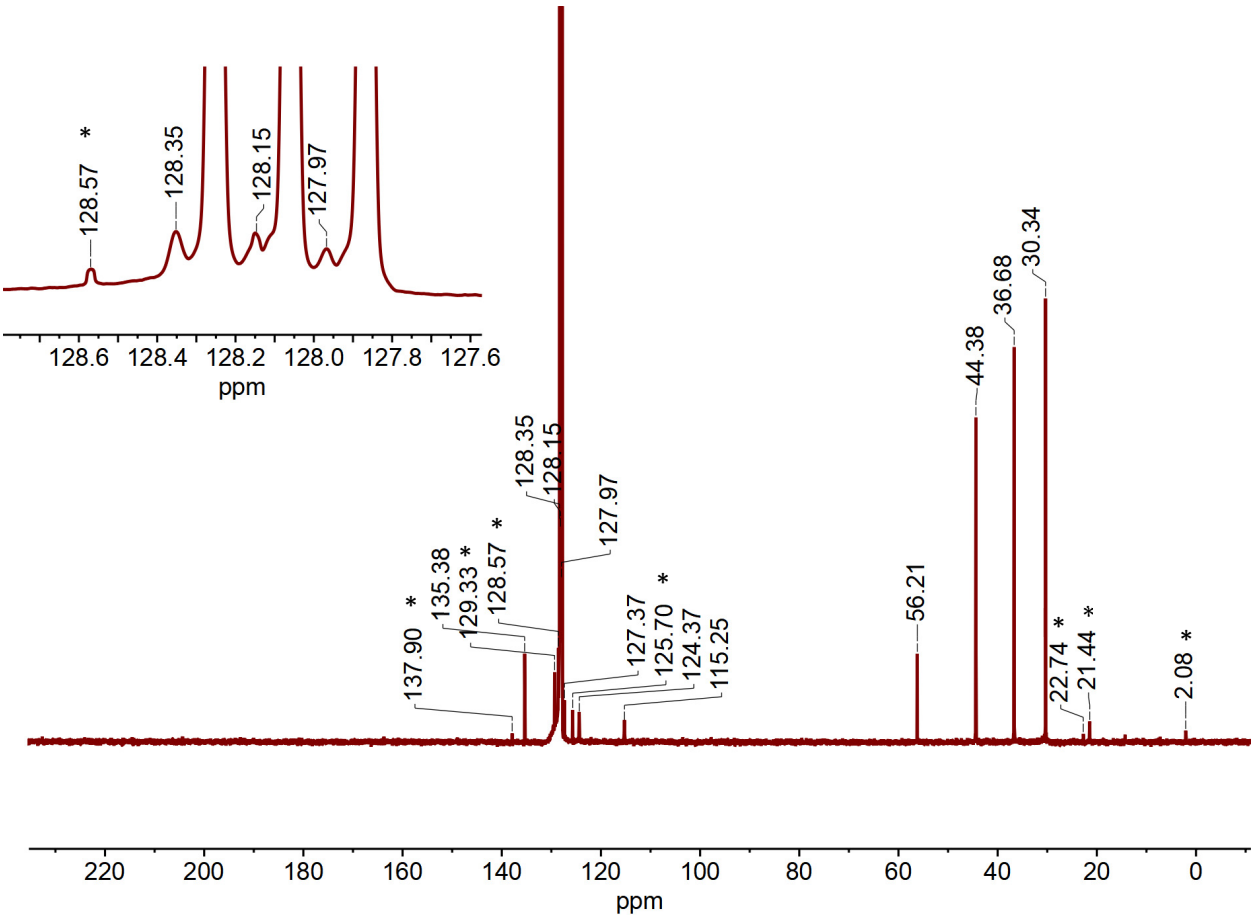

Figure S13. The ^{13}C NMR spectrum of **2b** in C_6D_6 at 298 K. Residual solvent peaks for toluene, pentane, and HMDSO marked with asterisks.

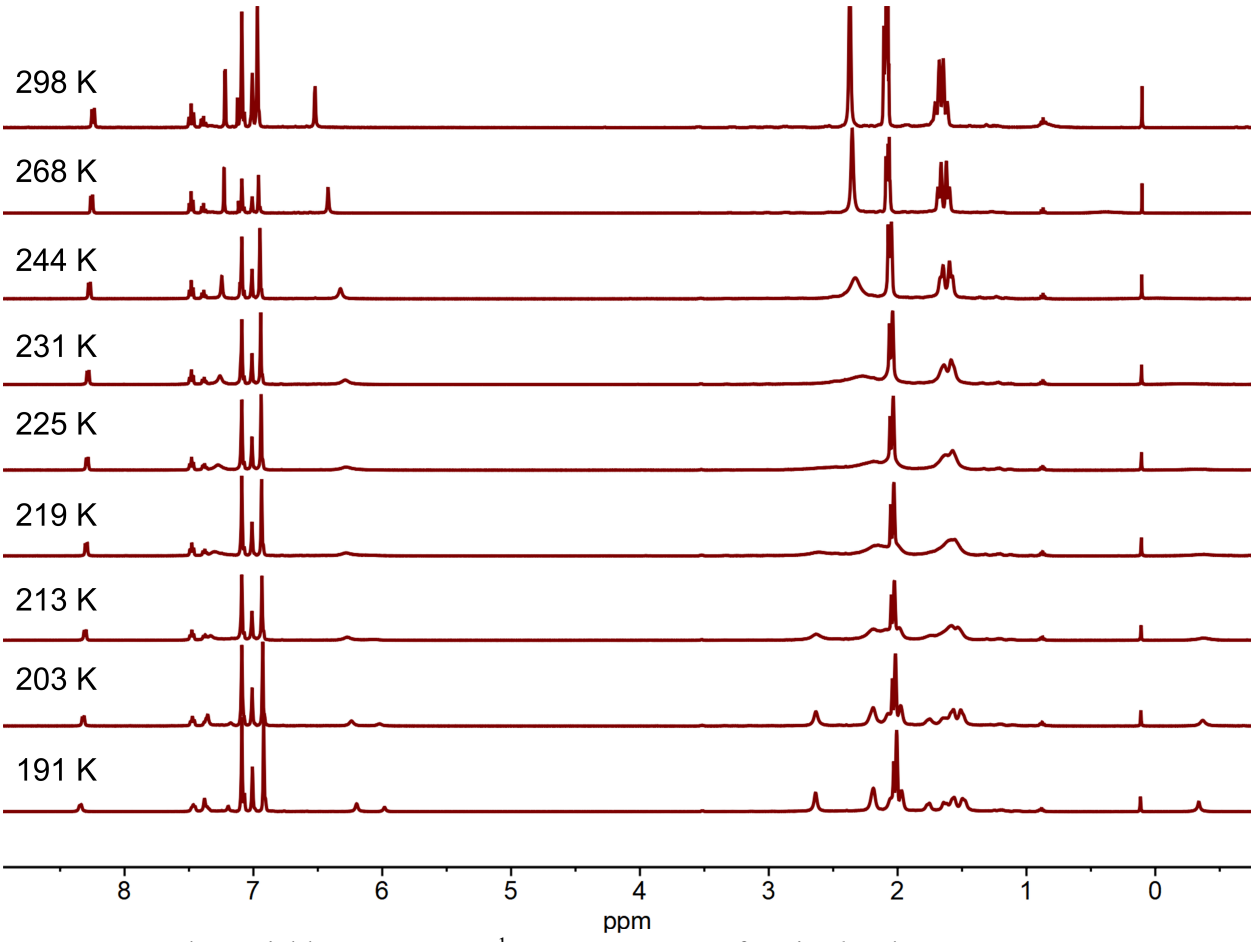

Figure S14. The variable temperature ^{1}H NMR spectra of **2b** in *d*$_{8}$-toluene.

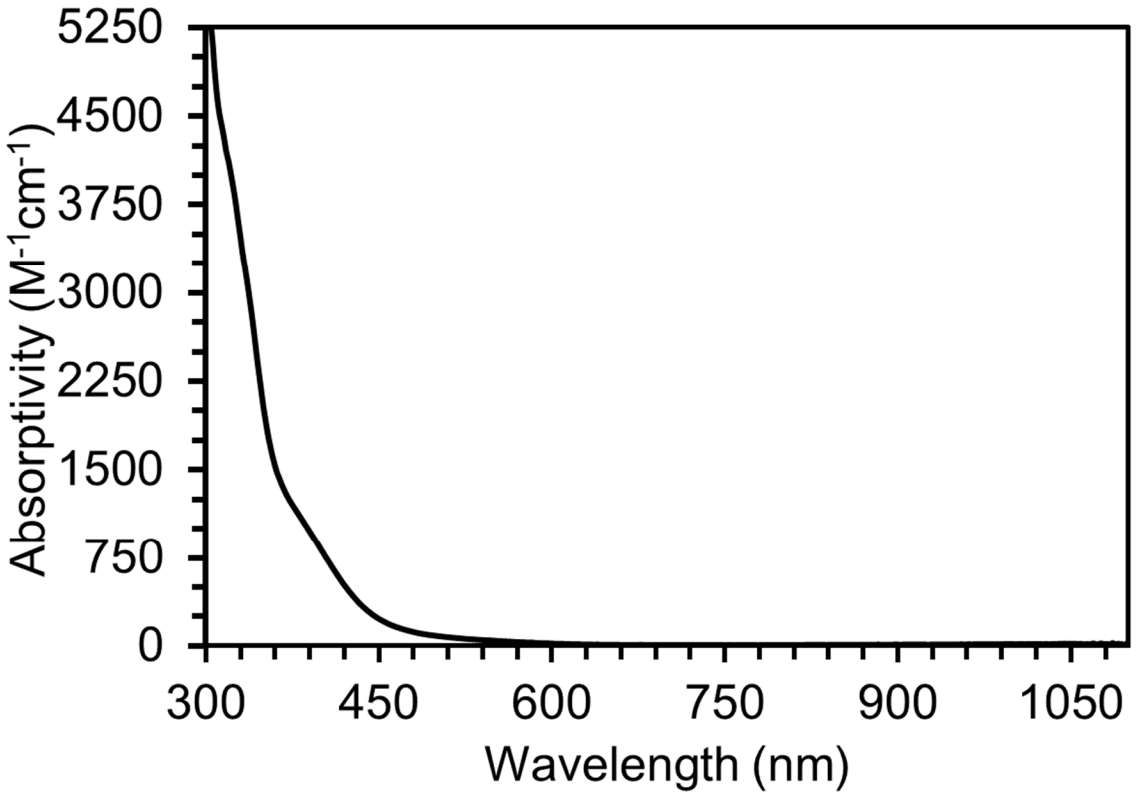

Figure S15. The UV-vis spectrum of **2b** in THF at 298 K.

Conformation	Free Energy Difference Relative to Optimized Singlet (kcal/mol)
Optimized Singlet	0
Triplet	+11
Singlet, linearized	+31

Table S2. Computed free energies of different conformations of **2a**. Note that "linearized" indicates the energy of a geometry optimization with a constrained B-Ni-C(Me) angle of 168°. Basis sets and functional listed in general procedures above.

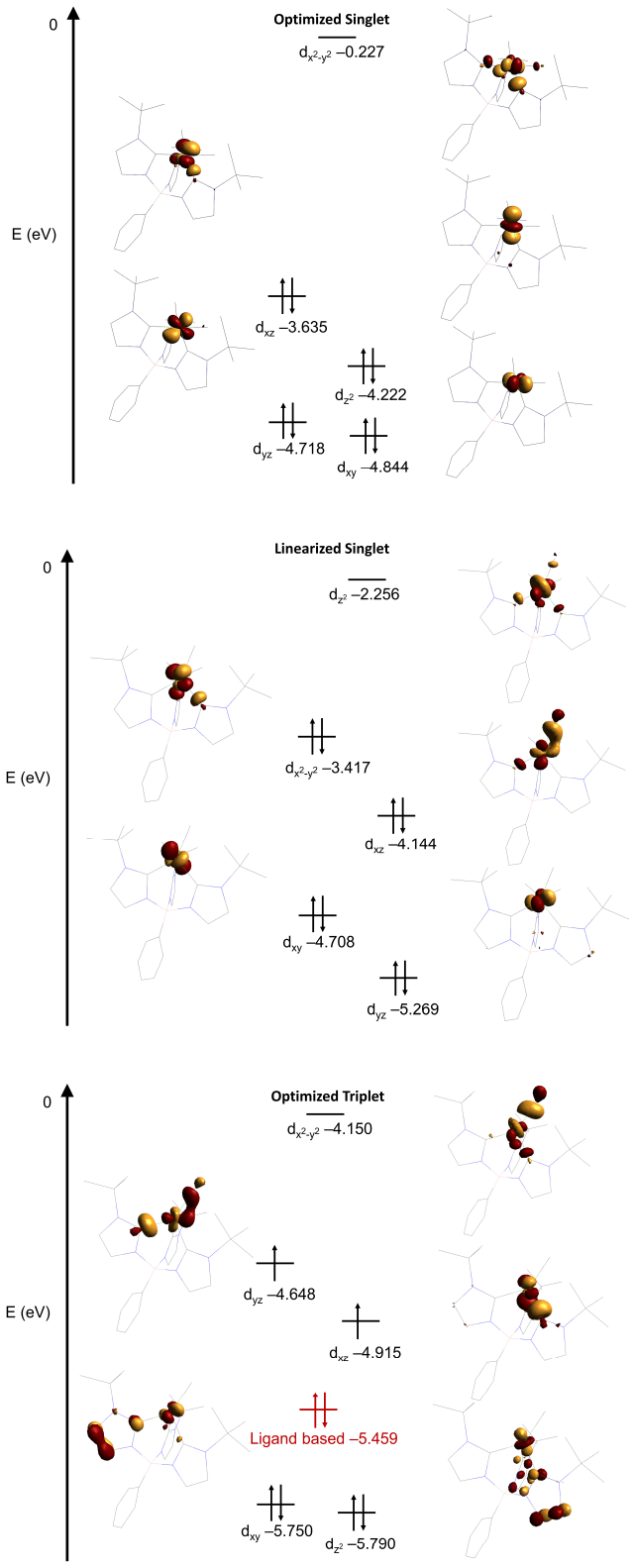

Figure S16. Kohn-Sham orbitals of **2a** in both seesaw (optimized singlet, top) and tetrahedral (linearized singlet, middle) geometries in a singlet electronic configuration, and optimized linear geometry in a triplet electronic configuration (bottom). Not to scale.

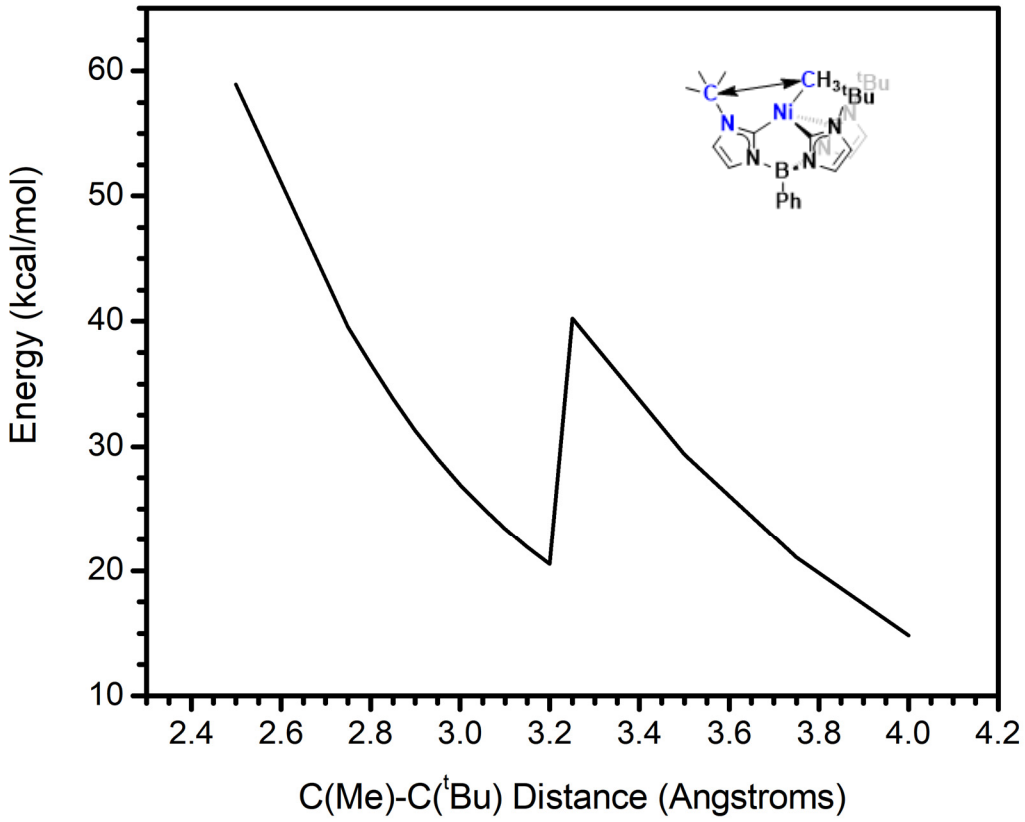

Figure S17. Plot of free energy on singlet manifold, scanning C(Me)-C(^{t}Bu) distance in **2a**. Constrained dihedral angle of blue atoms to 0º. Geometry scan run using BP86. Energies are relative to optimized singlet (BP86). These data were used to assess the viability of a lever mechanism in the isomerization of **2a**. Note that the discontinuity is associated with a reorganization of the ^{t}Bu and Me groups.

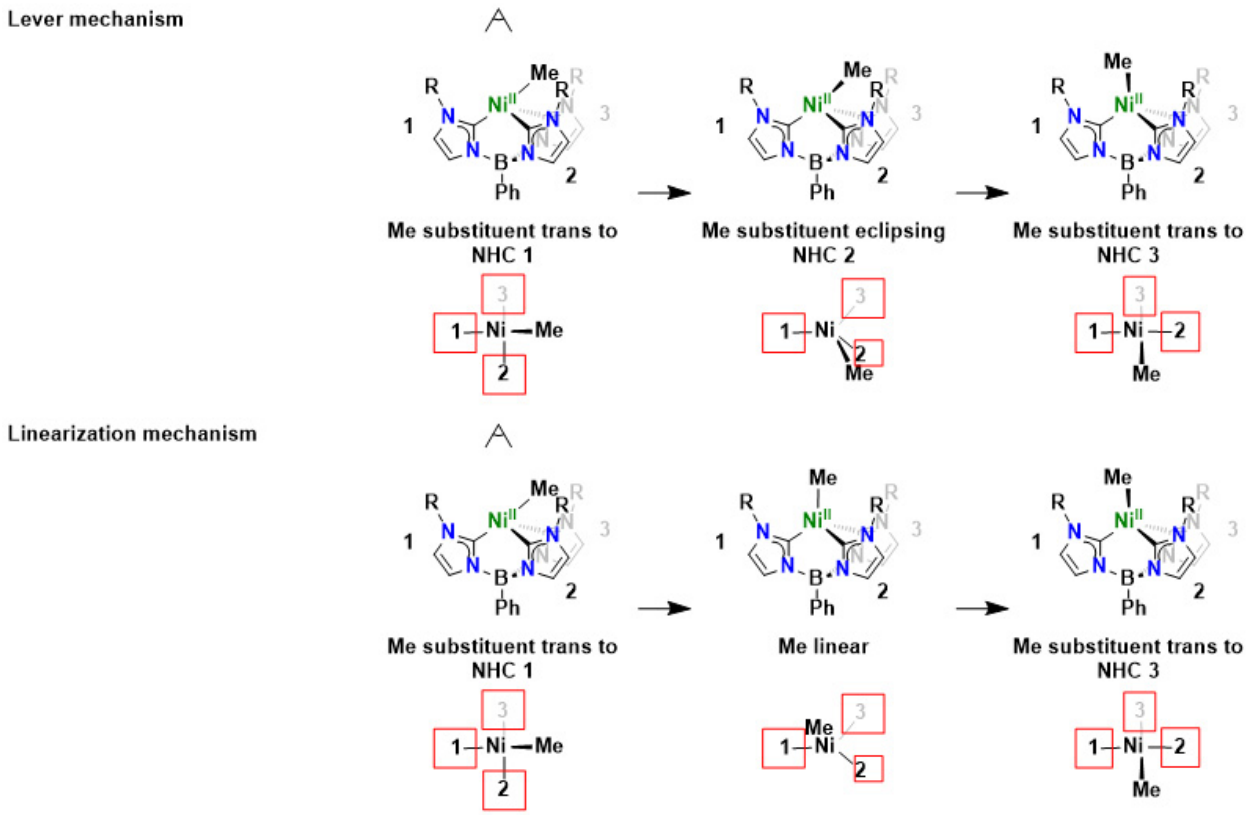

Figure S18. Pictorial representation of the lever and linearization mechanisms for isomerization of the Ni-Me complexes. NHC groups have been abbreviated as numbered boxes for top-down view.

O3LYP	BP86	B3LYP
10.9	13.0	1.2

Table S3. Triplet-singlet energy difference (kcal/mol) calculated for **2a** using different functionals.

Identification code	**1a**	**1b**	**2a**	**2b**
Empirical formula	$C_{27}H_{38}BClN_6Ni$	$C_{45.7}H_{57.4}BCl_{2.4}N_6Ni$	$C_{28}H_{41}BN_6Ni$	$C_{46}H_{59}BN_6Ni$
Formula weight	551.60	845.37	531.19	765.51
Temperature/K	100(2)	100(2)	100(2)	110(2)
Crystal system	monoclinic	monoclinic	triclinic	tetragonal
Space group	$P2_1/n$	$P2_1/n$	P-1	$I4_1/a$
a/Å	9.6383(16)	19.896(3)	9.8692(5)	34.481(3)
b/Å	17.821(3)	11.9883(15)	12.4359(7)	34.481(3)
c/Å	16.177(3)	21.333(3)	12.6239(7)	13.9826(14)
α/°	90	90	99.808(2)	90
β/°	91.925(6)	107.846(3)	97.233(2)	90
γ/°	90	90	113.118(2)	90
Volume/Å^3	2777.0(8)	4843.3(11)	1371.98(13)	16625(3)
Z	4	4	2	16
ρ_{calc}g/cm^3	1.319	1.159	1.286	1.223
μ/mm^{-1}	0.822	0.568	0.735	0.127
F(000)	1168.0	1790.0	568.0	6560.0
Crystal size/mm^3	0.48 × 0.28 × 0.19	0.35 × 0.31 × 0.21	0.298 × 0.295 × 0.153	0.03 × 0.03 × 0.03
Radiation	MoKα (λ = 0.71073)	MoKα (λ = 0.71073)	MoKα (λ = 0.71073)	synchrotron (λ = 0.41328)
2Θ range for data collection/°	4.572 to 50.148	4.78 to 50.81	4.504 to 55.016	1.374 to 32.464
Index ranges	$-11 \le h \le 11$, $-21 \le k \le 20$, $-19 \le l \le 19$	$-24 \le h \le 23$, $-14 \le k \le 14$, $-25 \le l \le 25$	$-12 \le h \le 12$, $-16 \le k \le 16$, $-16 \le l \le 16$	$-46 \le h \le 46$, $-46 \le k \le 46$, $-18 \le l \le 18$
Reflections collected	25048	59965	37813	252183
Independent reflections	4930 [R_{int} = 0.0560, R_{sigma} = 0.0487]	8900 [R_{int} = 0.0944, R_{sigma} = 0.0736]	6259 [R_{int} = 0.0424, R_{sigma} = 0.0366]	10760 [R_{int} = 0.0435, R_{sigma} = 0.0120]
Data/restraints/parameters	4930/0/334	8900/0/514	6259/0/335	10760/0/488
Goodness-of-fit on F^2	1.014	1.032	1.055	1.087
Final R indexes [I>=2σ (I)]	R_1 = 0.0385, wR_2 = 0.0847	R_1 = 0.1004, wR_2 = 0.2515	R_1 = 0.0345, wR_2 = 0.0691	R_1 = 0.0412, wR_2 = 0.0984
Final R indexes [all data]	R_1 = 0.0633, wR_2 = 0.0939	R_1 = 0.1419, wR_2 = 0.2746	R_1 = 0.0484, wR_2 = 0.0737	R_1 = 0.0434, wR_2 = 0.0997
Largest diff. peak/hole / e Å^{-3}	0.56/-0.23	1.31/-1.15	0.56/-0.33	0.49/-0.43

Table S4. Crystal structure refinement details for complexes **1a**, **1b**, **2a**, and **2b**.

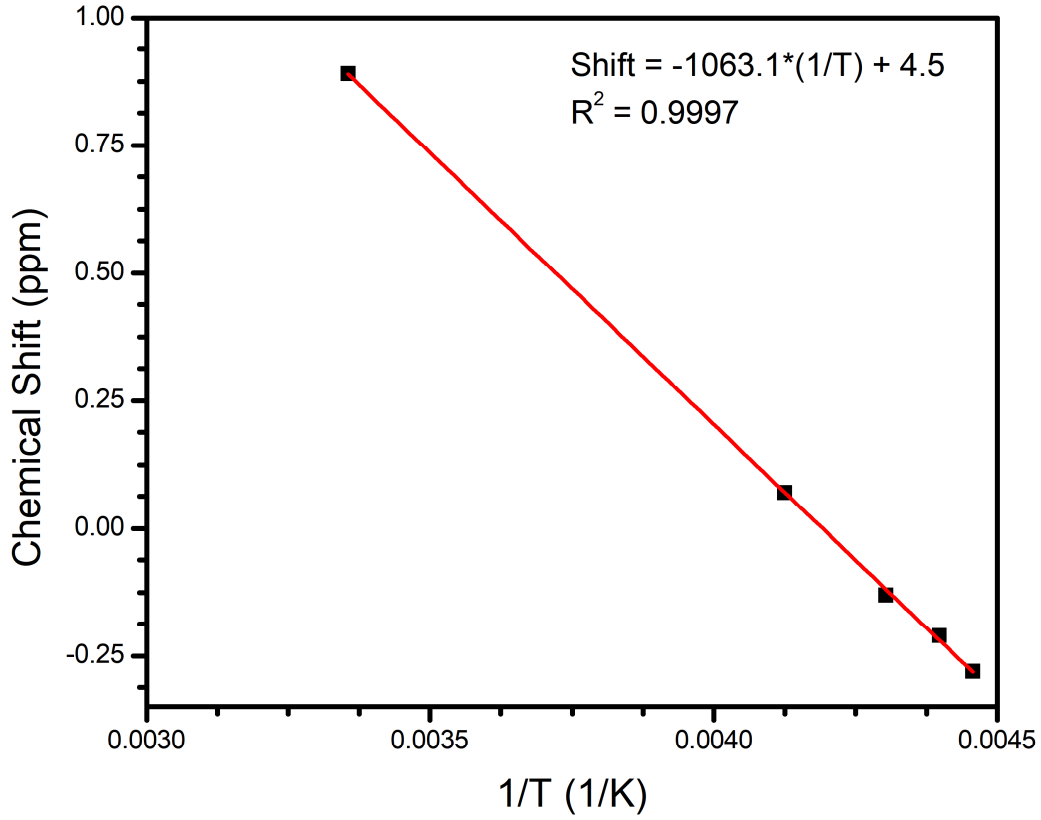

Figure S19. Plot of chemical shift versus 1/T for Ni-C*H*$_3$ resonance of **2a** in the fast exchange regime (T = 224-298 K).

References

1 N. S. Gill and R. S. Nyholm, *J. Chem. Soc.*, 1959, **0**, 3997.

2 R. E. Cowley, R. P. Bontchev, E. N. Duesler and J. M. Smith, *Inorg. Chem.*, 2006, **45**, 9771–9779.

3 Y. Xiong, S. Yao, T. Szilvási, E. Ballestero-Martínez, H. Grützmacher and M. Driess, *Angew. Chem., Int. Ed.*, 2017, **56**, 4333–4336.

4 Y. Fan, J. Cheng, Y. Gao, M. Shi and L. Deng, *Acta Chim. Sin.*, 2018, **76**, 445–452.

5 D. F. Evans, *J. Chem. Soc.*, 1959, 2003–2005.

6 G. M. Sheldrick, *SHELXTL*, 2014.

7 G. M. Sheldrick, *Acta Crystallogr.*, 2015, **A71**, 3–8.

8 G. M. Sheldrick, *Acta Crystallogr.*, 2015, **C71**, 3–8.

9 L. Krause, R. Herbst-Irmer, G. M. Sheldrick and D. Stalke, *J. Appl. Crystallogr.*, 2015, **48**, 3–10.

10 F. Neese, *Wiley Interdiscip. Rev. Comput. Mol. Sci.*, 2012, **2**, 73–78.

11 F. Weigend and R. Ahlrichs, *Phys. Chem. Chem. Phys.*, 2005, **7**, 3297–3305.

12 A. Schäfer, C. Huber and R. Ahlrichs, *J. Chem. Phys.*, 1994, **100**, 5829–5835.

13 A. Schäfer, H. Horn and R. Ahlrichs, *J. Chem. Phys.*, 1992, **97**, 2571–2577.

14 D. H. Putz and D. K. Brandenburg, *Diamond - Crystal and Molecular Structure Visualization, Crystal Impact*, GbR, Kreuzherrenstr. 102, 53227 Bonn, Germany.

15 M. D. Hanwell, D. E. Curtis, D. C. Lonie, T. Vandermeersch, E. Zurek and G. R. Hutchison, *J. Cheminform.*, 2012, **4**, 17.

16 H. Shanan-Atidi and K. H. Bar-Eli, *J. Phys. Chem.*, 1970, **74**, 961–963.

17 J. Sandström, *Dynamic NMR Spectroscopy*, Academic Press, London, 1982.